Chinese Journal of Chemical Engineering 76 (2024) 64–74

Contents lists available at ScienceDirect

Chinese Journal of Chemical Engineering

journal homepage: www.elsevier.com/locate/CJChE

Full Length Article

Numerical investigation of turbulent mass transfer processes in turbulent fluidized bed by computational mass transfer

Hailun Ren [1], Liang Zeng [2], Wenbin Li [2,*], Shuyong Chen [3], Zhongli Tang [4], Donghui Zhang [4]

[1] Department of Chemical Engineering, Tianjin Renai College, Tianjin 301636, China
[2] School of Chemical Engineering and Technology, Tianjin University, Tianjin 300072, China
[3] Innovation Center for Advanced Glass Materials (Anhui) Co., Ltd, Bengbu, 233000, China
[4] The Research Center of Chemical Engineering, School of Chemical Engineering and Technology, Tianjin University, Tianjin 300072, China

ARTICLE INFO

Article history:
Received 12 July 2024
Received in revised form
19 September 2024
Accepted 23 September 2024
Available online 11 October 2024

Keywords:
Turbulent fluidized bed
Simulation
Computational mass transfer
Turbulence
Computational fluid dynamics

ABSTRACT

Turbulent fluidized bed possesses a distinct advantage over bubbling fluidized bed in high solids contact efficiency and thus exerts great potential in applications to many industrial processes. Simulation for fluidization of fluid catalytic cracking (FCC) particles and the catalytic reaction of ozone decomposition in turbulent fluidized bed is conducted using the Eulerian–Eulerian approach, where the recently developed two-equation turbulent (TET) model is introduced to describe the turbulent mass diffusion. The energy minimization multi-scale (EMMS) drag model and the kinetic theory of granular flow (KTGF) are adopted to describe gas–particles interaction and particle–particle interaction respectively. The TET model features the rigorous closure for the turbulent mass transfer equations and thus enables more reliable simulation. With this model, distributions of ozone concentration and gas–particles two-phase velocity as well as volume fraction are obtained and compared against experimental data. The average absolute relative deviation for the simulated ozone concentration is 9.67% which confirms the validity of the proposed model. Moreover, it is found that the transition velocity from bubbling fluidization to turbulent fluidization for FCC particles is about 0.5 $m \cdot s^{-1}$ which is consistent with experimental observation.

1. Introduction

Compared with bubbling fluidization and fast fluidization, turbulent fluidization has a lot of advantages such as higher gas–solid contact efficiency, higher solid volume fraction and lower axial dispersion of gas. By virtue of these advantages make the turbulent fluidized bed become a promising multiphase reactor for the catalyst cracking, gasification, methanol-to-olefins (MTO) and combustion that involves strong exothermic reaction [1].

However, vigorous gas–solid interaction results in complex flow hydrodynamics including dramatic movement of particles and turbulence of both phases, which leads to great difficulty in experimental and theoretical analysis on turbulent fluidization, thereby hindering the design and optimization of turbulent fluidized bed [2]. Nevertheless, thanks to the substantial development of computer technology, numerical simulation (*i.e.*, computational fluid dynamics) can make complements to experimental and theoretical analysis while overcoming their limitations and is adopted as an effective way to investigate the gas–solid two-phase flow in turbulent fluidization process [3]. Generally, the gas phase is deemed as continuous phase and is treated under the Eulerian framework, whereas the solid phase is either regarded as continuous phase by Eulerian approach [4] or regarded as dispersed phase by Lagrangian approach [5]. Since trajectory of each particle should be tracked under Largrangian framework, it requires large amount of computer resources. Therefore, the treatment of solid phase as continuous by Eulerian approach is often used for fast simulation of numerous particles fluidization [3,6–8].

Since turbulent effect is significant in turbulent fluidization turbulence of gas and solid phase should be taken into account in mathematical model. There are several turbulent models for the multiphase flow in fluidized bed, including the standard k–ε model, k–ω model and the Reynolds stress model as well as their corresponding modified models. For instance, Zheng *et al.* [9] proposed a modified k–ε model, namely the $k_g - \varepsilon_g - k_p - \varepsilon_p - \Theta$ model, that incorporates the influence of particle clusters and

* Corresponding author.
E-mail address: richard@tju.edu.cn (W. Li).

https://doi.org/10.1016/j.cjche.2024.09.009

integrates the kinetic theory of granular flow (KTGF) for the particle stress. So far, this model has been applied to simulating various types of fluidized beds (*e.g.*, bubbling fluidized bed, circulating fluidized bed riser and downer) and satisfactory agreements are found between simulations and experiments [10–14]. As for the gas–solid two-phase interaction, there will be in need of an appropriate drag model. Conventional drag model such as the Ergun drag [15], the Wen–Yu drag [16] and their combination form as Gidaspow drag [4] are all obtained from experiments and mainly based on the assumption of homogeneously dispersed particle in system. However, it is found that heterogeneous structure of flow (*i.e.*, particle cluster and gas bubble) have significant influence on gas–solid interaction [17,18]. Therefore, many researchers have proposed modified drag models, *e.g.*, the energy minimization multi-scale based (EMMS) drag [19,20], the cluster structure dependent (CSD) drag [21] and the drag established by the transfer coefficient-based structural parameters (TC-SP) method [22].

As for the modeling of mass transfer process in turbulent fluidized bed, the closure for the species turbulent mass transfer equation or species conservation equation is needed. To our best knowledge, despite numerous studies on bubbling fluidized bed and circulating fluidized bed [23–27] where the turbulent mass diffusivity is determined by correlating with turbulent viscosity through turbulent Schmidt number model (*i.e.*, $Sc_t = \mu_t/\rho D_t$), researches on modeling of mass transfer process in turbulent fluidized bed (TFB) are far from enough to be dealt with. Furthermore, the right choice of turbulent Schmidt number from 0.7 to 1.1 is quiet dependent on experience and the constant turbulent Schmidt number itself is also questionable [10–14]. To resolve this uncertainty, Li *et al.* [10] introduced the $\overline{c^2} - \varepsilon_c$ model for the rigorous determination of turbulent mass diffusivity by two deduced model equations.

In this paper, simulations of a low velocity turbulent fluidized bed involving catalytic reaction on Geldart A group particles are conducted under the framework of Eulerian–Eulerian approach. The integrated $k_g - \varepsilon_g - k_s - \varepsilon_s - \Theta$ model by Zheng *et al.* [9] and the $\overline{c^2} - \varepsilon_c$ model by Li *et al.* [10] are applied to describing the two-phase turbulent flow coupled with the turbulent mass transfer process. While the bubble-based EMMS drag [20] is used for the two-phase interaction. Based on the comparison between the two data types, the result that the simulation results correspond with the experimental results is obtained. Furthermore, the microscale/macroscale flow and mass transfer behavior are characterized in terms of transient and time-averaged parameters including those of hydrodynamics and mass transfer process.

2. Modeling and Simulation

2.1. Simulation target

Experiments on ozone decomposition process in a TFB with fluid catalytic cracking (FCC) based catalyst by Liu and Zhu [28] are taken as target for modeling and simulation. As reported by Liu and Zhu [28] the TFB is 3 m in height and 152 mm in inner diameter. The FCC particle has an apparent density of 1780 $kg \cdot m^{-3}$ and a mean diameter of 78.6 μm. The ozone decomposition is a simple first order reaction and the thermal effect can be neglected because of the low ozone concentration (*i.e.*, inlet concentration of ozone is only 2×10^{-6} $kg \cdot m^{-3}$).

2.2. Model equations

The model to be used is established on the basis of the Eulerian–Eulerian approach, where both phases are deemed as penetrating continua. In mathematical expression, the model is composed by two parts including the species conservation equation along with its closure and the accompanied computational fluid dynamics part.

2.2.1. Species conservation equation

The conservation equation for species of ozone in gas is

$$\frac{\partial}{\partial t}\left(\rho_g \alpha_g \overline{C_i}\right) + \nabla\left(\rho_g \alpha_g \boldsymbol{u}_g \overline{C_i}\right) = \nabla\left(\rho_g \alpha_g D_{gi,e} \nabla \overline{C_i}\right) + R_i \tag{1}$$

$$\sum_i \overline{C_i} = 1$$

where the ρ_g, α_g and $\boldsymbol{u}_g$ are the density, volume fraction and velocity vector of gas phase respectively; $\overline{C_i}$ denotes the species mass fraction (*i.e.*, i = ozone, oxygen or the rest air); R_i is the sink or product of species caused by reaction; $D_{gi,e}$ is the species effective mass transfer diffusivity and is defined as:

$$D_{gi,e} = D_{gi} + D_{gi,t} \tag{2}$$

where D_{gi} and $D_{gi,t}$ are the molecule and turbulent mass diffusivity respectively. The turbulent mass diffusivity is often estimated roughly by using empirical correlation from experiments or by assuming a constant turbulent Schmidt number (*i.e.*, $D_{gi,t} = \mu_{g,t}/Sc_{gi,t}$). However, not only the assumption of a turbulent Schmidt number at the range of 0.7–1.1 is somewhat arbitrary, but also the constant value for turbulent Schmidt number is questionable since it is revealed that the turbulent Schmidt number is varied throughout the bubbling fluidized bed and circulating fluidized bed downer [10–14]. Thus, it is reckoned that the constant turbulent Schmidt number model might also produce deviations for the simulation of turbulent fluidized bed. Therefore, the rigorous $\overline{c^2} - \varepsilon_c$ two-equation turbulent (TET) model [10] is applied to determining the turbulent mass diffusivity $D_{gi,t}$ as follow [29]:

$$D_{gi,t} = C_{c_0} k_g \left[k_g \overline{c_i^2} \Big/ \left(\varepsilon_g \varepsilon_{c_i}\right)\right]^{1/2} \tag{3}$$

where k_g and ε_g are the turbulent kinetic energy and its dissipation rate that will be determined by the $k_g - \varepsilon_g - k_s - \varepsilon_s - \Theta$ model mentioned in the next section; the concentration variance $\overline{c_i^2}$ and its dissipation rate ε_{c_i} can be described by the following equations deduced by Liu [29] as:

$$\frac{\partial}{\partial t}\left(\alpha_g \rho_g \overline{c_i^2}\right) + \nabla \times \left(\alpha_g \rho_g \boldsymbol{u}_g \overline{c_i^2}\right) = \nabla \times \left[\left(D_{gi} + \frac{D_{gi,t}}{\sigma_c}\right)\alpha_g \nabla \overline{c_i^2}\right] + 2\rho_g \alpha_g \nabla \overline{C_i} \nabla \overline{C_i} - 2\rho_g \alpha_g \varepsilon_{c_i} \tag{4}$$

$$\frac{\partial}{\partial t}\left(\alpha_g \rho_g \varepsilon_{c_i}\right) + \nabla \times \left(\alpha_g \rho_g \boldsymbol{u}_g \varepsilon_{c_i}\right) = \nabla \times \left[\left(D_{gi} + \frac{D_{gi,t}}{\sigma_{\varepsilon_c}}\right)\rho_g \alpha_g \nabla \varepsilon_{c_i}\right] + C_{c_1} \rho_g \alpha_g \nabla \overline{C_i} \nabla \overline{C_i} \frac{\varepsilon_{c_i}}{\overline{c_i^2}} + C_{c_2} \rho_g \alpha_g \frac{\varepsilon_{c_i}}{k_g} \overline{\overline{\tau}_{g,t}} \nabla \boldsymbol{u}_g - C_{c_3} \rho_g \alpha_g \frac{\varepsilon_{c_i}^2}{\overline{c_i^2}} - C_{c_4} \rho_g \alpha_g \frac{\varepsilon_g \varepsilon_{c_i}}{k_g} + D_{gi} D_{gi,t} \left(\frac{\partial^2 \overline{C_i}}{\partial x_i \partial x_j}\right)^2 \tag{5}$$

where the constants in Eqs. (3)–(5) are [29,30]: $C_{c_0} = 0.11$, $C_{c_1} = 1.80$, $C_{c_2} = 1.40$, $C_{c_3} = 2.20$, $C_{c_4} = 0.80$, $\sigma_c = 1.0$ and $\sigma_{\varepsilon_c} = 1.0$.

The source term R_i in Eq. (1) representing the decomposition rate of ozone R_{O_3} or the formation rate of oxygen R_{O_2} and can be calculated by

$$R_{O_3} = -r\frac{P_g}{R_g T_g}M_{O_3}\ ,\ R_{O_2} = +r\frac{P_g}{R_g T_g}M_{O_2} \tag{6}$$

where the P_g, T_g and R_g are gas phase pressure, temperature and universal constant; M_{O_3}, M_{O_2} denote the ozone/oxygen molar mass; r represents the catalytic decomposition rate that can be determined by $r = k_r X_{O_3}\alpha_s$; X_{O_3} is the molar concentration of ozone; α_s is the solids holdup and k_r is the constant of catalytic decomposition rate that can be determined from experiment in a fixed bed reactor.

2.2.2. Computational fluid dynamics part

The computational fluid dynamics part of the model consists of the governing equations, *i.e.*, the continuity and momentum equations of gas and solid phase, and the constitutive equations, *i.e.*, the $k_g-\varepsilon_g-k_s-\varepsilon_s-\Theta$ model equations [9] for the turbulent flow of two-phase and the interaction inner solid phase. As for the drag model describing interaction between gas and solid phase, the EMMS based drag is adopted considering the dramatic interaction and the existence of particle clusters in turbulent fluidization. Detailed expressions for the $k_g-\varepsilon_g-k_s-\varepsilon_s-\Theta$ model and the EMMS drag model are summarized in Supplementary Material, and interested readers can also refer to related literatures elsewhere [9,20].

The above computational fluid dynamics part equations integrated with the species conservation equation and its $\overline{c^2}-\varepsilon_c$ closure form the proposed model for the turbulent fluidized bed involving ozone catalytic decomposition.

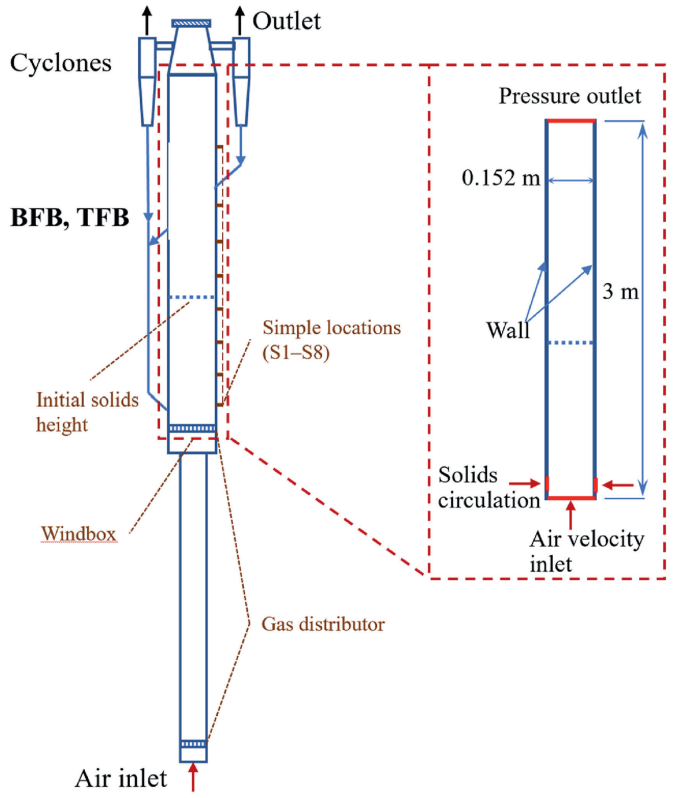

Fig. 1. Boundary condition arrangements for the simulated turbulent fluidized bed, bubbling fluidized bed (BFB). (S1–S8 in Supplementary Material)

2.3. Numerical procedures

Boundaries of the computation domain are shown in Fig. 1. The simulation target, a turbulent fluidized bed, is a part of the multi-functional experiment set for fluidization as established by Zhu's group [28]. The specific boundary conditions are arranged as follow. The bottom inlet conditions including the gas flow rate and the inlet concentration of ozone are set the same as those of the experiments, while in setting the $k_g-\varepsilon_g-k_s-\varepsilon_s-\Theta$ as well as the $\overline{c^2}-\varepsilon_c$ methods of Li *et al.* [10] are adopted. The outlet of the TFB is set to be pressure-outlet. At the wall, the no-slip and partial-slip conditions [31] are taken for the gas and particles respectively. It is noteworthy that at high gas flow rate the particles may flow out of the bed and will return to the bed bottom after separated by the upper cyclone. By hooking a user-defined function to record the particles flux at the top outlet and particles return to the bottom inlet boundary, the circulation of the particles is realized in simulation.

The commercial software Gambit 2.4.6 is used to mesh the computation domain of the TFB, and the software Ansys Fluent 14.5 (2D) is used to carry out the simulation for finding the numerical solutions of the model equations. The detailed setting in meshing and simulation are summarized in Table 1. It should be mentioned that the independent analysis of mesh and time-step sizes are made and the detailed procedures are similar with our previous work [11,12]. Generally, refining the grid size can guarantee more accurate numerical simulation. For fluidized bed simulation, Agrawal *et al.* [34] suggested the grid size of about 10 times the particle diameter is sufficient, whilst Wang *et al.* [6] found that simulation results are far less sensitive to grid size if the sub-grid scale structural effect is taken into consideration which is the situation of this work where the EMMS drag is used. In this paper, grid sizes of 1, 2 and 4 mm are used (*i.e.*, about 13, 25 and 51 times the particle diameter) to implement the grid size independence test. Fig. 2 illustrates the comparison of simulated solids concentration

Table 1
Materials properties, main operating conditions and numerical settings for the simulation.

Particle properties	Density, ρ_s/kg·m^{-3}	1780
	Diameter, d_s/μm	78.6
Gas properties	Gas density, ρ_g/kg·m^{-3}	1.2
	Gas shear viscosity, μ_g/Pa·s	1.8×10^{-5}
Operating conditions	Initial solids height, H_0/m	1.0
	Superficial gas velocity, U_g/m·s^{-1}	0.3–0.8
	Inlet ozone concentration/ kg·m^{-3}	2.0×10^{-6}
Numerical settings	Transient formulation	First order implicit
	Pressure velocity coupling	Phase coupled SIMPLE
	Momentum discretization	Second order upwind
	Volume fraction discretization	Quick
	Turbulent mass diffusion model	Li *et al.* [10], Sc_t
	Turbulent viscous model	Zheng *et al.* [9]
	Granular temperature	Zheng *et al.* [9]
	Granular viscosity	Gidaspow [4]
	Granular bulk viscosity	Lun *et al.* [32]
	Frictional viscosity	Schaeffer [33]
	Solids pressure	Lun *et al.* [32]
	Radial distribution	Lun *et al.* [33]
	Gas–particle drag	EMMS [20], Gidaspow [4]
	Angle of internal friction	30
	Packing limit, $\alpha_{s,max}$	0.63
	Restitution coefficient, e_{pp}, $e_{pi,j}$	0.9
	Grid size/mm	2
	Time step size/s	2×10^{-4}
	Residual criterion	1×10^{-5}

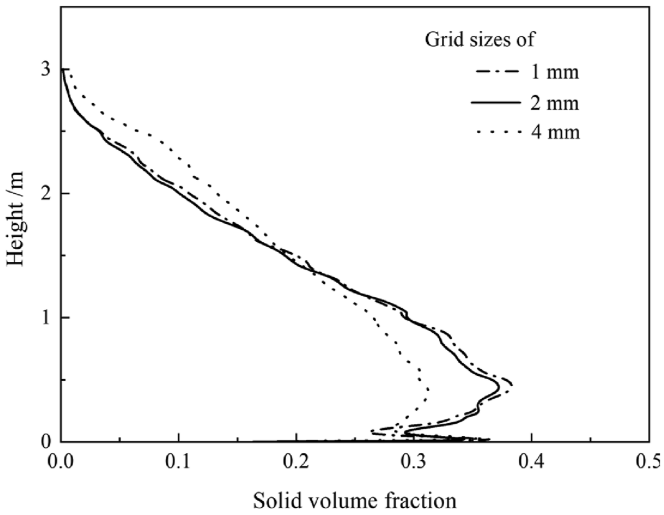

Fig. 2. Simulated solids volume fraction profiles under different mesh schemes for the case of $U_g = 0.8\ m \cdot s^{-1}$.

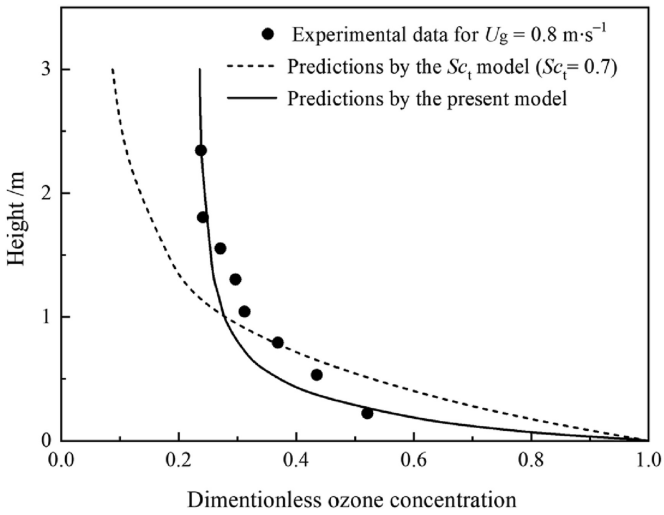

Fig. 3. Comparisons of ozone concentration distributions between simulated results and experimental data.

profiles between using different grid sizes. It is seen that the grid size beyond 2 mm results in significant deviations whilst the finer grid with size of 1 mm only leads to slight difference in simulation. Therefore, grid size of 2 mm is chosen for all simulation cases.

3. Results and Discussions

3.1. Time-averaged characteristics

Due to the non-linear-non-equilibrium characteristics of such system, the multiphase flow as well as the involved mass transfer process are chaotic in fluidization especially in turbulent fluidization [35]. In this section, the time-averaged characteristics are shown for the purpose of analyzing the macroscale features of the turbulent fluidization in terms of axial and radial profiles of parameters in hydrodynamics flow and mass transfer process.

3.1.1. Profiles of ozone concentration

A profound understanding of the characteristics of mass transfer process is of great importance in designing and optimizing a fluidized bed reactor, while the species concentration distribution reflects directly the efficiency of the reactor. Therefore, for the sake of discussing the mass transfer behavior in the TFB it is essential to depict the distributions of the species. Fig. 3 shows the axial profiles of ozone concentration in the TFB, where the circles represent the experimental data and the lines are simulated results by different models. It is illustrated that encouraging simulation results on ozone concentration (as depicted by solid line) are obtained by the present TET model [10] while the results by the Sc_t model deviate largely from the experimental measurements, which indicates the capability of the TET model in simulating TFB involving reactive flow process. Fig. 4 depicts the time-averaged contour of ozone concentration. It is seen from this figure that the turbulent mass diffusion affects the mass transfer process and species concentration distributions significantly. The empirical method for determination of turbulent mass diffusivity by a constant Sc_t number would cause obvious simulation errors (*i.e.*, the average absolute relative deviation, AARD, between simulations by TET model and experiments on ozone concentration distribution is about 9.67%. While the AARD% for the Sc_t number model is up to 29.4%). Detailed discussions about the characteristic of turbulent mass diffusion as well as its effect on mass transfer behavior and chemical reaction will be made in later section (see Section 3.1.3).

3.1.2. Profiles of solids volume fraction and gas–solid two phases velocities

Fig. 5 gives time-averaged solids volume fraction contours by the $k_g - \varepsilon_g - k_s - \varepsilon_s - \Theta$ model with the EMMS drag [9,20] and the Gidaspow drag [4], respectively. Both drag models predict a core–annual like solids concentration distribution, whereas the dense–dilute phase distribution pattern in the bottom and top regions are much different as a denser phase is seen in the bottom region by the EMMS drag than that by the Gidaspow drag, as shown in Fig. 6(a). It can be understood that the Gidaspow drag would overestimate the gas–solids interaction force as have been reported in previous works [11,12,36], therefore solids even flow out of the TFB top. It should be noted that by hooking a UDF to record the particles flux at the top outlet and particles return to the bottom inlet boundary, the circulation of the particles is realized in simulation, as described in Section 2.3.

Fig. 6(b) and (c) also provide the simulated results for experiment at different operating conditions (superficial gas velocity, U_g). All the simulations show a deviation near the bottom region, which should be attributed to the 2D assumption where the wall effect or constrain of flow would be underestimated when comparing with the real 3D situation, thus less solids may be accumulated at the bottom region [12,37]. Despite the deviations of the simulations near the bottom region, the overall agreement between the simulations by the present model and the experimental data is satisfactory as shown in Fig. 6 where the average absolute relative deviation, AARD, of the present model for the case of $U_g = 0.8\ m \cdot s^{-1}$ is about 10.8%, which suggests that the 2D assumption is sufficient for the present TFB simulation. However, the AARD of the Gidaspow drag is up to 70% due to lack of well consideration for meso structure effect on multiphase flow in turbulent fluidization. It is worth mentioning that though the EMMS drag ensures much better simulation of TFB in terms of solids concentration profile, the combination of EMMS drag and Sc_t model fails in predicting the mass transfer process since a large simulation error is found as provided in Section 3.1.1. It indicates that the closure method for the differential turbulent mass transfer equation for species of ozone (see Eq. (1) in Section 2) has significant influence on simulation of mass transfer process. And the

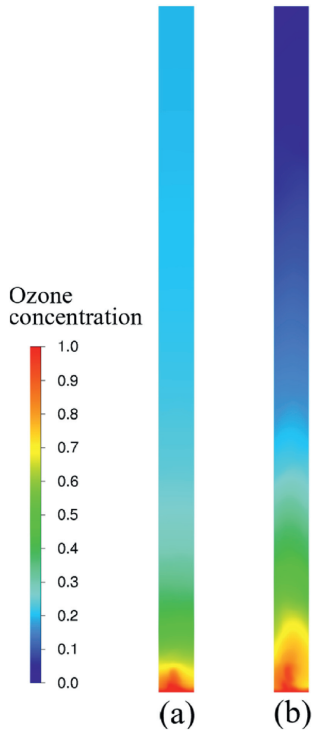

Fig. 4. Simulated contours of ozone concentration by different models: (a) TET model predictions and (b) Sc_t model predictions.

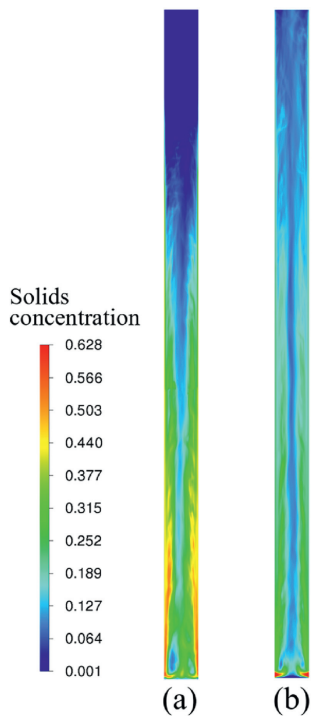

Fig. 5. Simulated time-averaged contours of solids volume fraction: (a) EMMS drag predictions and (b) Gidaspow drag predictions.

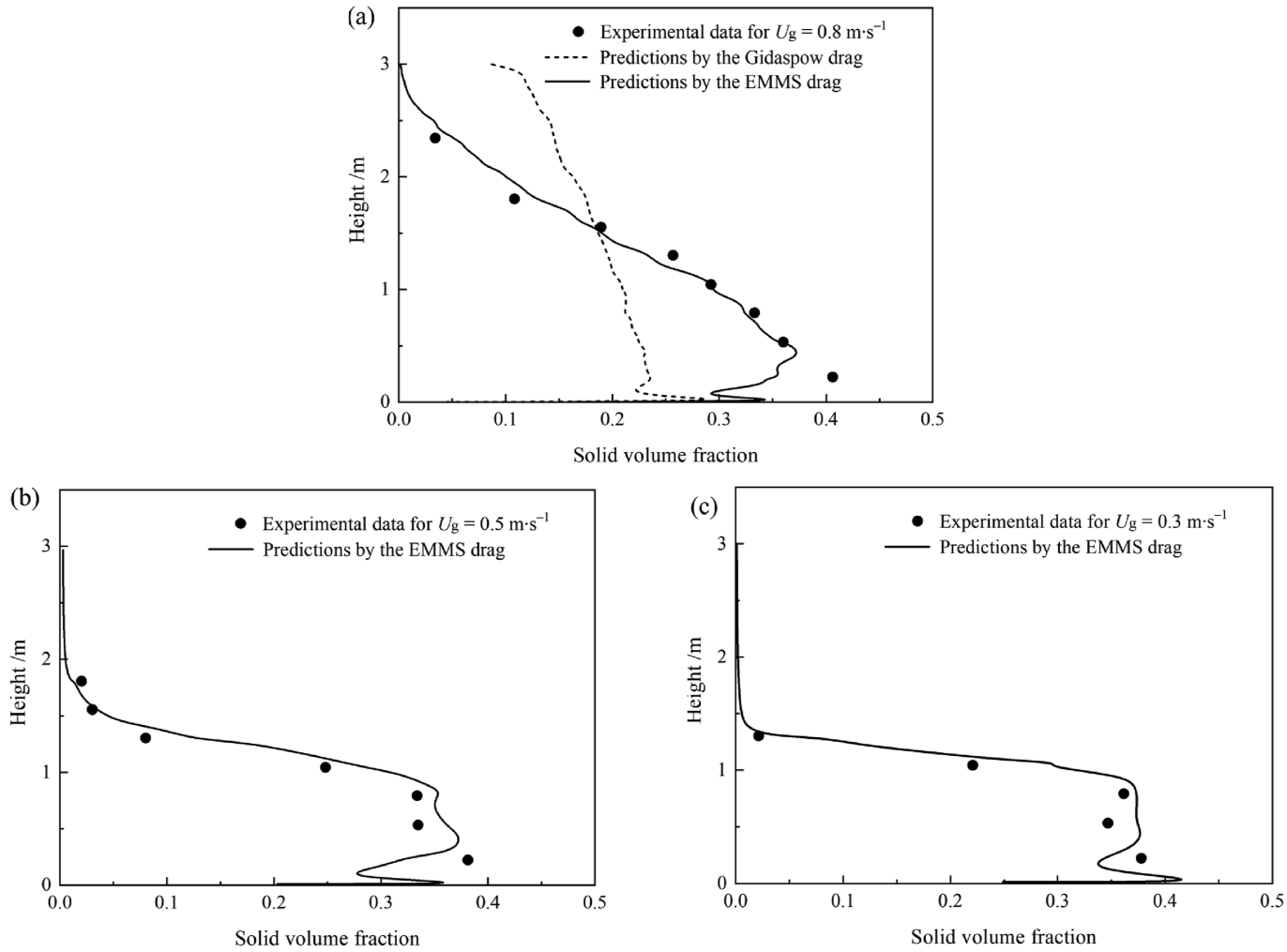

Fig. 6. Comparisons of solids volume fraction distributions between simulated results and experimental data.

proposed TET model for the closure of Eq. (1) shows its advantage over Sc_t number model in simulation of TFB involving mass transfer process.

Fig. 7 illustrates the radial distributions of solids concentration, where the predictions at different bed heights (*i.e.*, the solid lines) agree well with the experimental data displayed as solid symbols. It is also found that the core–annual structure of the solid concentration simulated by the proposed model is consistent with the experimental observation. Fig. 8(a) and (b) show the radial profiles of gas and solids velocities respectively. The gas velocity is found to be reducing gradually, even flowing downward when $|r/R|$ is beyond 0.5, and dropping to zero because of the no-slip condition of the wall. The distribution of solids phase velocity has the similar pattern with that of gas phase but the solids phase velocity is somewhat slower than the gas one. And the solids phase velocity in vicinity of the wall will not be constrained to zero since the partial-slip condition of the wall is applied.

3.1.3. *Profiles of turbulent mass diffusivity*

As seen in Fig. 9 the value of turbulent mass diffusivity is up to 10^{-1} m^2·s^{-1}, indicating more significant turbulent mass

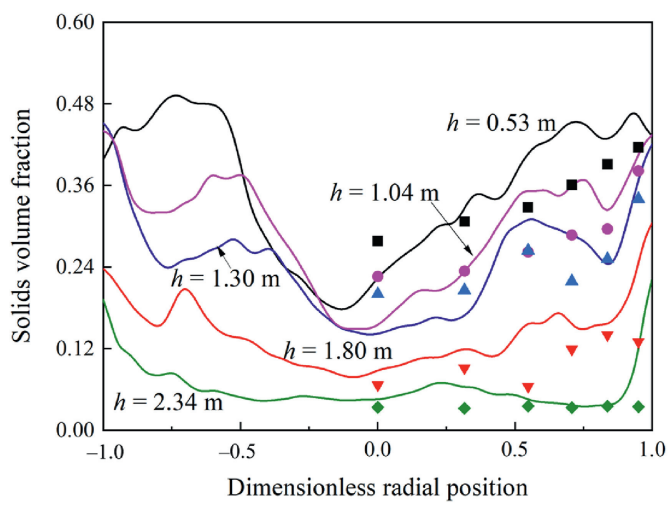

Fig. 7. Simulated radial profiles of solids volume fraction at different bed height.

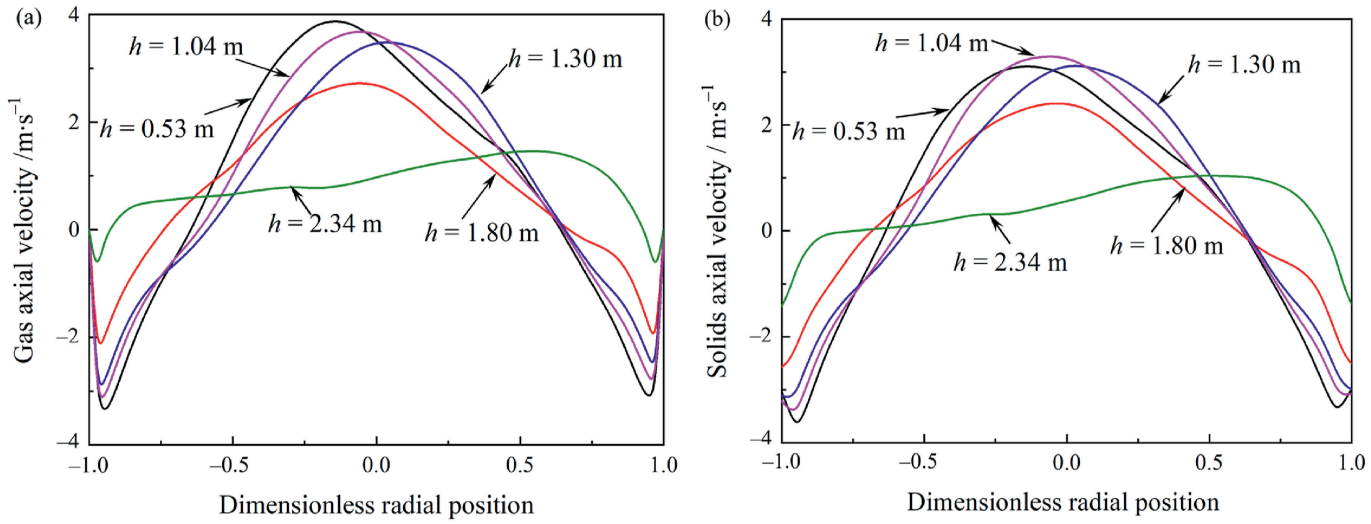

Fig. 8. Simulated radial profiles of phase velocity at different bed heights: (a) for gas phase and (b) for solids phase.

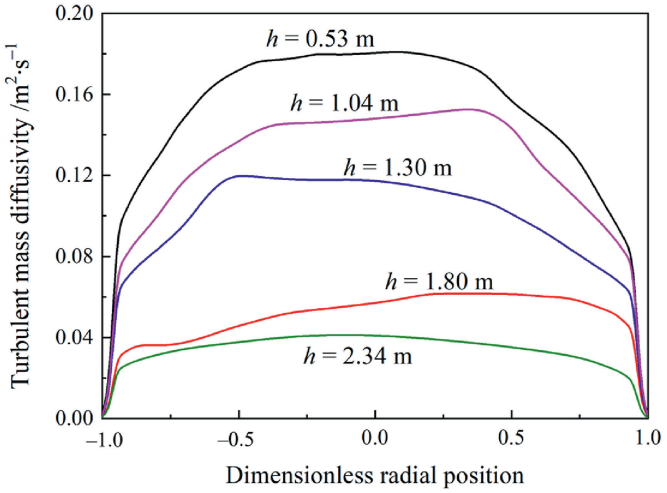

Fig. 9. Radial profiles of turbulent mass diffusivity at different bed height.

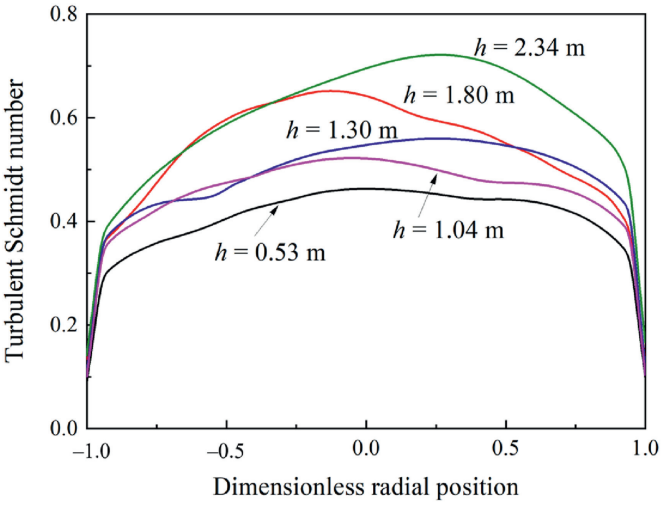

Fig. 10. Radial profiles of turbulent Schmidt number at different heights.

diffusion in the TFB than in other type of fluidized bed [10–12]. The turbulent mass diffusivity is found to be higher in the bottom than that in the upper region, which should be due to the following reasons: i) the gas phase velocity distribution is dramatically changes from a uniform pattern (as set for the inlet boundary) to a parabolic shape shortly after entering the TFB. The quick change of phase velocity may enhance the turbulent flow induced turbulent mass diffusion. ii) the ozone concentration is also undergoing changes more significantly at the lower part of the TFB as seen in Fig. 3, which leads to higher gradient of species concentration. As have been found in our previous studies, higher change of species concentration would also result in more significant turbulent mass diffusion [10–12]. At a specific height, the value of turbulent mass diffusivity is higher in the center region and decreased to zero at the wall surface. This can be explained by the wall effect since non-slip condition is applied at the wall surface where both turbulent flow and the created turbulent mass diffusion are constrained.

Fig. 10 illustrates the turbulent Schmidt number ($Sc_{g,t} = \mu_{g,t}/(\rho_g \cdot D_{g,t})$) obtained by the proposed TET model. It should be noted that in the present simulation the turbulent Schmidt number is not required. Here the provided profiles of $Sc_{g,t}$ is only served to show that it is not a constant in the entire TFB but is varied from bottom to top and from center to near wall regions. It also explains that the use of constant $Sc_{g,t}$ produces significant simulation errors as shown in Fig. 3. Further explanations should be that the use of constant 0.70 for the empirical turbulent Schmidt number model

leads to underestimation of turbulent mass diffusivity according to the correlation of $D_{g,t} = \mu_{g,t}/(\rho_g \cdot Sc_{g,t})$ since the overall averaged turbulent Schmidt number obtained by the present model is found to be about 0.53. And lower values of turbulent mass diffusivity mean less significant axial back-mixing or dispersion of ozone, resulting in underestimation of the adverse effect of mixing on reactor performance (*i.e.*, less intensive mixing leads to relative higher ozone concentration in the bottom part of the TFB and relative lower concentration in the upper part), and consequently, the first-order catalytic reaction rate in the bottom part would be relative overestimated as expressed by Eq. (6). Therefore, higher conversion or lower concentration of ozone at reactor exit is obtained by the empirical turbulent Schmidt number model as shown in Fig. 3.

3.2. Transient characteristics

Due to the aforementioned non-linear-non-equilibrium characteristics of turbulent fluidization, the parameters in hydrodynamics may fluctuate dramatically with time. It is important to analyze the microscale features of the turbulent fluidization in terms of local fluctuating parameters, since the essential differences in local fluctuation play a key role in many aspects of fluidization, such as identifying and characterizing fluidization regimes.

Fig. 11(a), (b) and (c) display the transient solids concentration within 5 s at the center of the TFB (h = 1.04 m) for different operating conditions (U_g = 0.3, 0.5 and 0.8 m·s^{-1}). All of the results show obvious fluctuations whilst the frequency increases when superficial gas velocity increases from 0.3 to 0.5 m·s^{-1}. Continuous increase of the U_g from 0.5 to 0.8 m·s^{-1} only makes a slight difference in frequency of fluctuation. The time-averaged solids concentration under different superficial gas velocity are given as red dash lines in Fig. 11, where higher superficial gas velocity is found to result in lower time-averaged solids concentration since much more particles are carried upward. Fig. 12 illustrates the standard deviation of transient solids concentration versus superficial gas velocity at different radial positions (r/R = 0, 0.707 and 0.950). No obvious relation between the standard deviation of solids concentration and gas velocity can be observed since different tendencies are found in different radial positions. However, if the standard deviation of solids concentration is correlated with local

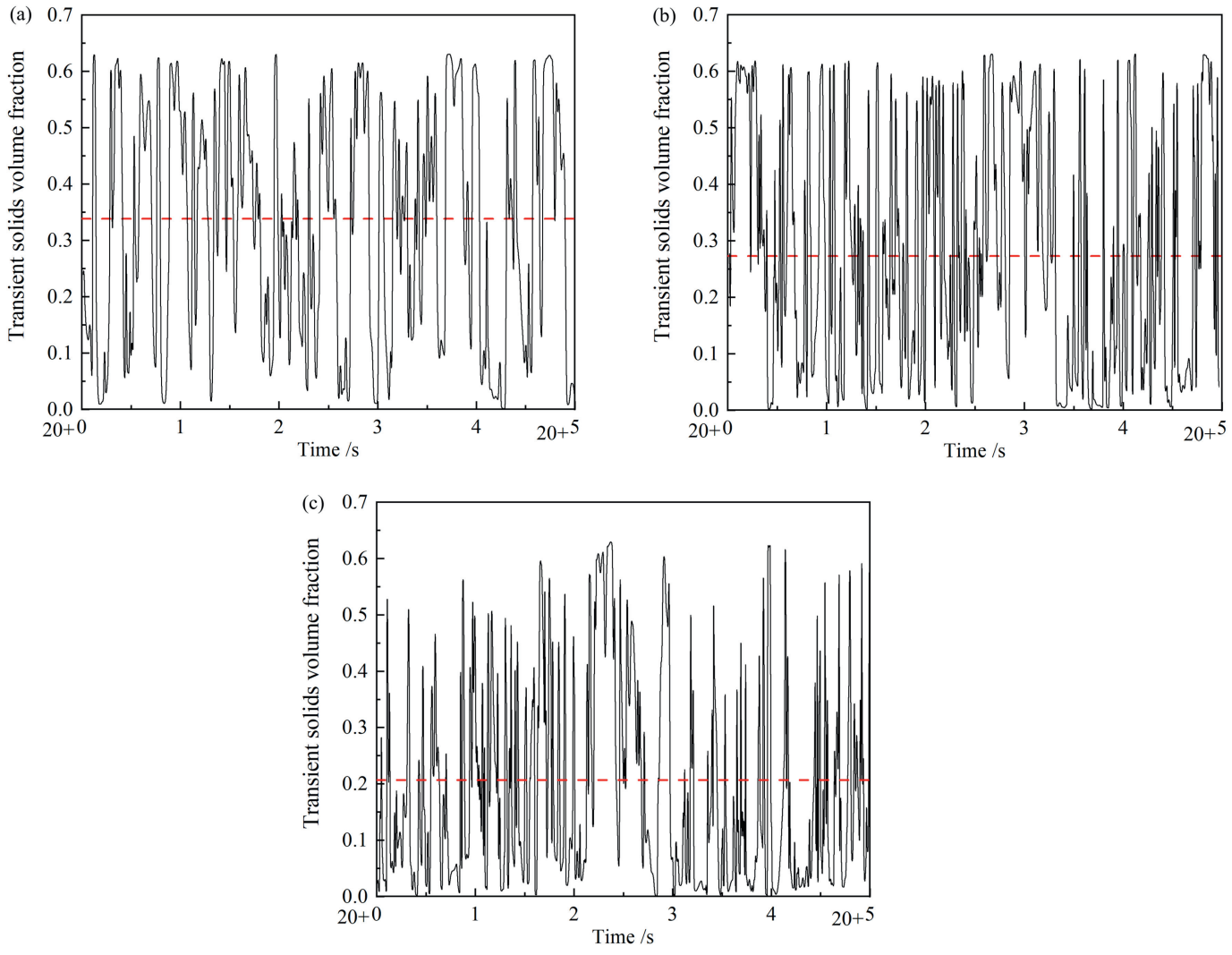

Fig. 11. Transient solids concentrations under different superficial gas velocities: (a) U_g = 0.3 m·s^{-1}, (b) U_g = 0.5 m·s^{-1}, and (c) U_g = 0.8 m·s^{-1}.

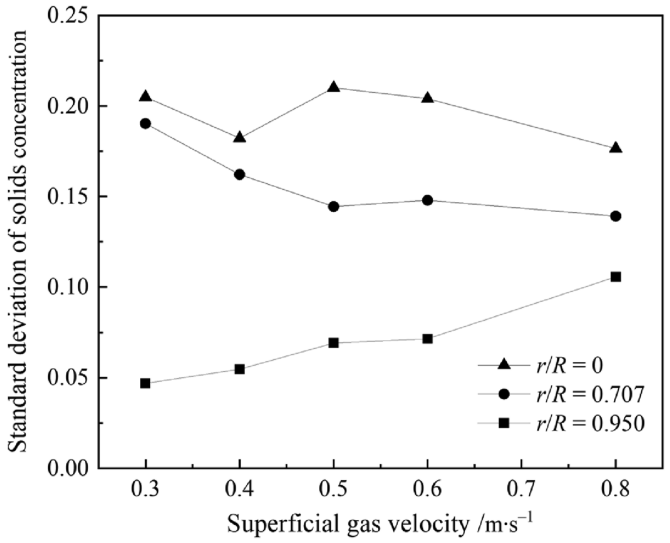

Fig. 12. Standard deviations of solids volume fraction versus superficial gas velocity.

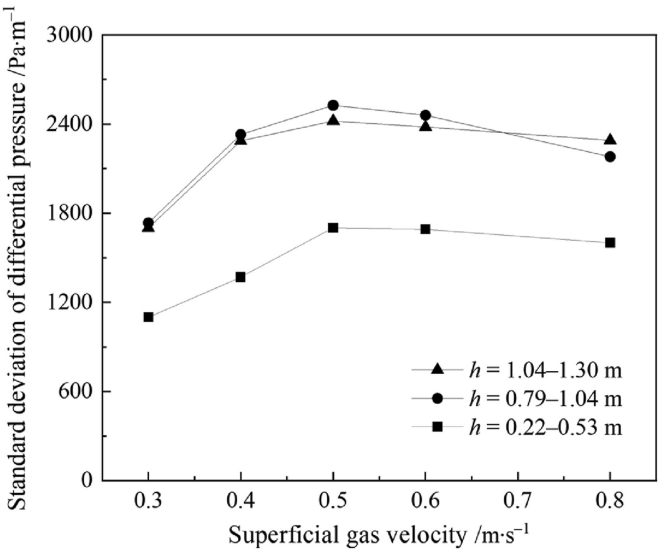

Fig. 14. Standard deviations of differential pressure at different heights.

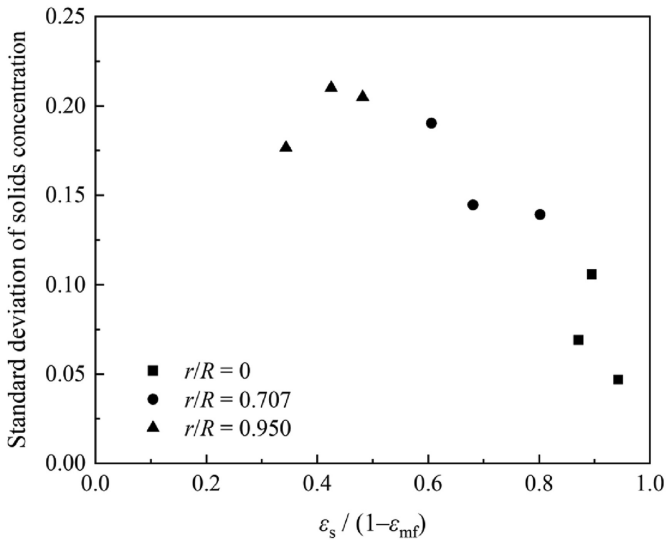

Fig. 13. Standard deviations of solids volume fraction versus solids concentration.

mean averaged solids concentration, as shown in Fig. 13, it is seen that despite a non-monotonicity of standard deviation of solids concentration (ε_{SD}) with the mean solids concentration is found, one can observe that the ε_{SD} is decreased when solids concentration approaches either 0 or $\varepsilon_{s,mf}$ (*i.e.*, the solids concentration at minimum fluidization ($1-\varepsilon_{mf}$)). Such findings agree well with the simulation results by Wang [6] and the experimental results by Issangya [38] and Bi and Su [39].

As shown in Fig. 14, the standard deviation of differential pressure at different bed heights displays a consistent trend of first increasing and then decreasing with increase of gas superficial velocity. As stated by Yerushalmi and Cankurt [40] the superficial gas velocity at which the standard deviation of differential pressure reaches its maximum (*i.e.*, $U_g = 0.5$ m·s^{-1}) is referred as the transition velocity from the bubbling fluidization regime to the turbulent fluidization regime. This finding also agrees with the experimental result by Liu and Zhu [28]. It is noted that the exact transition velocity is difficult to be determined since the regime transition from bubbling fluidization to turbulent fluidization is generally a gradual, not an abrupt process during gas velocity increases as have been stated by Liu *et al.* [41]. Herein, the obtained transition velocity is not that accurate due to the limited simulations but should be around $U_g = 0.5$ m·s^{-1} as depicted in Fig. 14.

4. Conclusions

The TET model is integrated with the $k_g - \varepsilon_g - k_p - \varepsilon_p - \Theta$ model for the simulation of a TFB involving ozone decomposition process. The TET model features the rigorous closure for the species conservation equation by the auxiliary $\overline{c^2} - \varepsilon_c$ two-equation, thereby enables more reliable predictions on mass transfer processes in TFB. Ozone concentration and gas–particle two-phase velocity as well as volume fraction distributions can be obtained simultaneously by the present integrated model. After comparing with experimental data, the following main conclusions can be made: (1) The simulated ozone concentration and solids concentration distributions agree well with the experimental measurements, which confirms that the proposed TET model is suitable for the simulation of TFB with chemical reaction. (2) The turbulent Schmidt number ($Sc_{g,t}$) is found to be varied throughout the TFB, which suggests that assumption of $Sc_{g,t}$ to be a constant is only an approximation. And the comparisons of ozone concentration distributions by different models illustrate that significant error would be produced by the conventional turbulent Schmidt number model (*i.e.*, $Sc_{g,t} = 0.7$), which implies the important influence of turbulent mass diffusion exerting on mass transfer process. (3) The use of EMMS drag makes the prediction on solids volume fraction distribution agree better with experiments than that by the Gidaspow drag mainly due to the overestimation of gas–particle interaction force by the Gidaspow drag. The results on standard deviation of differential pressure for different gas velocity suggest that the transition velocity from bubbling to turbulent fluidization of Geldart A particle is about 0.5 m·s^{-1}. And higher gas velocity would lead to higher frequency of solids concentration fluctuation.

CRediT Authorship Contribution Statement

Hailun Ren: Writing – original draft, Software, Investigation. Liang Zeng: Writing – review & editing, Methodology, Formal analysis. Wenbin Li: Writing – review & editing, Project administration, Funding acquisition. Shuyong Chen: Validation, Data curation. Zhongli Tang: Resources, Methodology. Donghui Zhang: Validation, Supervision, Conceptualization.

Declaration of Competing Interest

The authors declare that they have no known competing financial interests or personal relationships that could have appeared to influence the work reported in this paper.

Acknowledgements

The authors acknowledge the financial support from the National Natural Science Foundation of China (22078230), the National Key Research and Development Program of China (2023YFB4103600) and the State Key Laboratory of Heavy Oil Processing (SKLHOP202202008).

Supplementary Material

Supplementary data to this article can be found online at https://doi.org/10.1016/j.cjche.2024.09.009.

Nomenclature

C_{c_0}, C_{c_1}, C_{c_2}, C_{c_3}, C_{c_4}	turbulence model constants for the concentration field
C_q	mass fraction of species in phase q
$\overline{c^2}$	concentration variance
D_g	molecular diffusivity, $m^2 \cdot s^{-1}$
$D_{g,t}$	turbulent mass diffusivity, $m^2 \cdot s^{-1}$
H	total height of the TFB reactor, m
h	height of the TFB accounted from the bottom inlet, m
P_g	gas phase pressure, kPa
R	diameter of the TFB, m
r	radial distance from the TFB axis, m
S_{C_i}	source terms
Sc_t	turbulent Schmidt number
t	time, s
U_g	superficial velocity of the gas phase, $m \cdot s^{-1}$
$\boldsymbol{u}_g$, $\boldsymbol{u}_s$	gas and particle velocity vector, $m \cdot s^{-1}$
α_g, α_s	gas and solid volume fraction, respectively
ε_c	dissipation rate of the concentration variance, s^{-1}
ρ_g, ρ_s	gas and particle density, $kg \cdot m^{-3}$
σ_ε, $\sigma_{\varepsilon c}$, σ_t, $\sigma_{\varepsilon t}$	turbulence model constants

References

[1] H.T. Bi, N. Ellis, I.A. Abba, J.R. Grace, A state-of-the-art review of gas–solid turbulent fluidization, *Chem. Eng. Sci.* 55 (21) (2000) 4789–4825.
[2] J.R. Grace, Reflections on turbulent fluidization and dense suspension upflow, *Powder Technol.* 113 (3) (2000) 242–248.
[3] J. Chang, Z.J. Wu, X. Wang, W.Y. Liu, Two- and three-dimensional hydrodynamic modeling of a pseudo-2D turbulent fluidized bed with Geldart B particle, *Powder Technol.* 351 (2019) 159–168.
[4] D. Gidaspow, Multiphase Flow and Fluidization: Continuum and Kinetic Theory Descriptions, Academic Press, New York, 1994.
[5] S. Yuu, H. Nishikawa, T. Umekage, Numerical simulation of air and particle motions in group-B particle turbulent fluidized bed, *Powder Technol.* 118 (1–2) (2001) 32–44.
[6] J.W. Wang, Flow structures inside a large-scale turbulent fluidized bed of FCC particles: Eulerian simulation with an EMMS-based sub-grid scale model, *Particuology* 8 (2) (2010) 176–185.
[7] S. Benzarti, H. Mhiri, H. Bournot, R. Occelli, Numerical simulation of turbulent fluidized bed with Geldart B particles, *Adv. Powder Technol.* 25 (6) (2014) 1737–1747.
[8] A. Ullah, K. Hong, S. Chilton, W. Nimmo, Bubble-based EMMS mixture model applied to turbulent fluidization, *Powder Technol.* 281 (2015) 129–137.
[9] Y. Zheng, X.T. Wan, Z. Qian, F. Wei, Y. Jin, Numerical simulation of the gas–particle turbulent flow in riser reactor based on k–ε–k_p–ε_p–Θ two-fluid model, *Chem. Eng. Sci.* 56 (24) (2001) 6813–6822.
[10] W.B. Li, K. Yu, B.T. Liu, X.G. Yuan, Computational fluid dynamics simulation of hydrodynamics and chemical reaction in a CFB downer, *Powder Technol.* 269 (2015) 425–436.
[11] W.B. Li, Y.W. Zhang, Y.Y. Shao, J. Zhu, A rigorous model for the simulation of chemical reaction in gas–particle bubbling fluidized bed: I. Modeling and validation, *Powder Technol.* 327 (2018) 399–407.
[12] H.L. Ren, H.D. Zhang, W.B. Li, Z.L. Tang, D.H. Zhang, Simulation of CO_2 capture process in gas–solid bubbling fluidized bed by computational mass transfer, *J. Environ. Chem. Eng.* 10 (5) (2022) 108548.
[13] H.L. Ren, W.B. Li, L. Zeng, K.L. Liu, Z.L. Tang, D.H. Zhang, Numerical study on hydrodynamics of gas–solids circulating fluidized bed with L-valve, *Particuology* 77 (2023) 37–46.
[14] H.L. Ren, L. Zeng, W.B. Li, Z.L. Tang, D.H. Zhang, Numerical study on the hydrodynamics of a chemical looping combustion system with a binary-particle mixture, *Ind. Eng. Chem. Res.* 62 (38) (2023) 15675–15686.
[15] S. Ergun, Fluid flow through packed columns, *Chem. Eng. Prog.* 48 (1952) 89–94.
[16] C.Y. Wen, Y.H. Yu, Mechanics of fluidization, *Chem. Eng. Prog. Symp. Ser.* 62 (1966) 100–111.
[17] S. Zimmermann, F. Taghipour, CFD modeling of the hydrodynamics and reaction kinetics of FCC fluidized-bed reactors, *Ind. Eng. Chem. Res.* 44 (26) (2005) 9818–9827.
[18] D.Z. Zhang, W.B. VanderHeyden, The effects of mesoscale structures on the macroscopic momentum equations for two-phase flows, *Int. J. Multiphas. Flow* 28 (5) (2002) 805–822.
[19] J.W. Wang, W. Ge, J.H. Li, Eulerian simulation of heterogeneous gas–solid flows in CFB risers: EMMS-based sub-grid scale model with a revised cluster description, *Chem. Eng. Sci.* 63 (6) (2008) 1553–1571.
[20] K. Hong, Z.S. Shi, W. Wang, J.H. Li, A structure-dependent multi-fluid model (SFM) for heterogeneous gas–solid flow, *Chem. Eng. Sci.* 99 (2013) 191–202.
[21] S. Wang, H.L. Lu, G.D. Liu, Z.H. Sheng, P.F. Xu, D. Gidaspow, Modeling of cluster structure-dependent drag with Eulerian approach for circulating fluidized beds, *Powder Technol.* 208 (1) (2011) 98–110.
[22] W.M. Liu, H.Z. Li, Q.S. Zhu, Q.H. Zhu, A new structural parameters model based on drag coefficient for simulation of circulating fluidized beds, *Powder Technol.* 286 (2015) 516–526.
[23] L.M. Armstrong, S. Gu, K.H. Luo, P. Mahanta, Multifluid modeling of the desulfurization process within a bubbling fluidized bed coal gasifier, *AIChE J.* 59 (6) (2013) 1952–1963.
[24] V. Silva, E. Monteiro, N. Couto, P. Brito, A. Rouboa, Analysis of syngas quality from Portuguese biomasses: an experimental and numerical study, *Energy Fuels* 28 (9) (2014) 5766–5777.
[25] J. Xie, W.Q. Zhong, B.S. Jin, Y.J. Shao, H. Liu, Simulation on gasification of forestry residues in fluidized beds by Eulerian–Lagrangian approach, *Bioresour. Technol.* 121 (2012) 36–46.
[26] J.H. Chen, G.B. Yu, B. Dai, D. Liu, L. Zhao, CFD simulation of a bubbling fluidized bed gasifier using a bubble-based drag model, *Energy Fuels* 28 (10) (2014) 6351–6360.
[27] J. Chang, K. Zhang, Y.P. Yang, B.D. Wang, Q. Sun, Computational investigation of solid sorbent carbon dioxide capture in a fluidized bed reactor, *Powder Technol.* 275 (2015) 94–104.
[28] J.S. Liu, J. Zhu, Experimental study on reactor performance of gas–solids low-velocity fluidized beds, *Particuology* 66 (2022) 21–28.
[29] B.T. Liu, Study of a New Mass Transfer Model of CFD and its Application on Distillation Tray, Ph.D. Thesis, Tianjin University, China, 2003. (in Chinese)
[30] Y.S. Zhang, Turbulence, National Defense Industry Press, Beijing, 2002. (in Chinese)
[31] P.C. Johnson, R. Jackson, Frictional–collisional constitutive relations for granular materials, with application to plane shearing, *J. Fluid Mech.* 176 (1987) 67.
[32] C.K.K. Lun, S.B. Savage, D.J. Jeffrey, N. Chepurniy, Kinetic theories for granular flow: inelastic particles in Couette flow and slightly inelastic particles in a general flowfield, *J. Fluid Mech.* 140 (1984) 223–256.
[33] D.G. Schaeffer, Instability in the evolution equations describing incompressible granular flow, *J. Differ. Equ.* 66 (1987) 61–74.
[34] K. Agrawal, P.N. Loezos, M. Syamlal, S. Sundaresan, The role of meso-scale structures in rapid gas–solid flows, *J. Fluid Mech.* 445 (2001) 151–185.
[35] J.H. Li, M. Kwauk, Exploring complex systems in chemical engineering—the multi-scale methodology, *Chem. Eng. Sci.* 58 (3–6) (2003) 521–535.
[36] H.D. Zhang, W.B. Li, Q. Ma, Y.W. Zhang, F.L. Lei, Numerical study on influence of exit geometry in gas–solid flow hydrodynamics of HDCFB riser by CPFD, *Adv. Powder Technol.* 31 (9) (2020) 4005–4017.
[37] P.F. Ren, Y.W. Zhang, W.B. Li, K. Yu, Turbulent mass transfer model for simulating protein desorption in liquid–solid circulating fluidized bed risers, *Particuology* 57 (2021) 167–175.
[38] A.S. Issangya, Flow Dynamics in High Density Circulating Fluidized Beds, Ph.D. Thesis, The University of British Columbia, Canada, 1998.

[39] H.T. Bi, P.C. Su, Local phase holdups in gas−solids fluidization and transport, *AIChE J.* 47 (9) (2001) 2025−2031.
[40] J. Yerushalmi, N.T. Cankurt, Further studies of the regimes of fluidization, *Powder Technol.* 24 (2) (1979) 187−205.
[41] X.H. Liu, S.W. Hu, Y.F. Jiang, J.H. Li, Extension and application of energy-minimization multi-scale (EMMS) theory for full-loop hydrodynamic modeling of complex gas−solid reactors, *Chem. Eng. J.* 278 (2015) 492−503.